Ocean Sci. Discuss., 12, 1145–1186, 2015
www.ocean-sci-discuss.net/12/1145/2015/
doi:10.5194/osd-12-1145-2015

Ocean Science
Discussions
Open Access

How essential are Argo observations to constrain a global ocean data assimilation system?

V. Turpin[1,*], **E. Remy**[1], **and P. Y. Le Traon**[1,2]

[1]Mercator Ocean, Parc Technologique du Canal, 8–10 rue Hermès, 31520 Ramonville Saint Agne, France
[2]IFREMER, Technopôle Brest Iroise, Z.I de la Pointe du Diable, 29280 Plouzané, France
[*]now at: LOCEAN, Institut Pierre Simon Laplace, 4, place Jussieu 75252 Paris, France

Received: 12 March 2015 – Accepted: 24 April 2015 – Published: 22 June 2015

Correspondence to: V. Turpin (vtlod@locean-ipsl.upmc.fr)

Published by Copernicus Publications on behalf of the European Geosciences Union.

Abstract

Observing System Experiments (OSEs) are carried out over a one-year period to quantify the impact of Argo observations on the Mercator-Ocean 1/4° global ocean analysis and forecasting system. The reference simulation assimilates sea surface temperature (SST), SSALTO/DUACS altimeter data and Argo and other in situ observations from the Coriolis data center. Two other simulations are carried out where all Argo and half of Argo data sets are withheld. Assimilating Argo observations has a significant impact on analyzed and forecast temperature and salinity fields at different depths. Without Argo data assimilation, large errors occur in analyzed fields as estimated from the differences when compared with in situ observations. For example, in the 0–300 m layer RMS differences between analyzed fields and observations reach 0.25 psu and 1.25 °C in the western boundary currents and 0.1 psu and 0.75 °C in the open ocean. The impact of the Argo data in reducing observation-model forecast error is also significant from the surface down to a depth of 2000 m. Differences between independent observations and forecast fields are thus reduced by 20 % in the upper layers and by up to 40 % at a depth of 2000 m when Argo data are assimilated. At depth, the most impacted regions in the global ocean are the Mediterranean outflow and the Labrador Sea. A significant degradation can be observed when only half of the data are assimilated. All Argo observations thus matter, even with a 1/4° model resolution. The main conclusion is that the performance of global data assimilation systems is heavily dependent on the availability of Argo data.

1 Introduction

Argo is the first ever real-time global in situ ocean observing system. The initial target of 3000 profiling floats drifting in the ocean was reached by the international Argo program in November 2007. Mean coverage is one float in every 3°×3° box. Every 10 days, floats sample temperature and salinity from the surface to 2000 m and deliver data in real

OSD
12, 1145–1186, 2015

time, mostly for operational oceanography. Rigorous scientific quality control is applied by data operators in delayed time to guarantee optimal quality for this dataset (e.g. Cabanes et al., 2010; Wong et al., 2010). The use of Argo data is widespread in the ocean and climate research communities. Argo also provides critical observations to constrain ocean analysis and forecasting systems, together with satellite observations.

Operational oceanography capabilities have improved dramatically since the end of the 1990s thanks to the development of real time in situ and satellite global observing systems (in particular Argo and satellite altimetry) and the improvement of modelling and data assimilation techniques (e.g. Bell et al., 2009). Data assimilation techniques now provide efficient tools for analyzing the impact and optimizing the design of Global Ocean Observing Systems (GOOS) (e.g. Fujii et al., 2015; Lea et al., 2014).

The OceanObs09 conference held in Venice in September 2009 for the international coordination of interdisciplinary ocean observation highlighted the need to consolidate and improve the design of the global ocean observing system (Lindstrom et al., 2012). To meet this requirement, it is crucial to evaluate and quantify how the existing observation system constrains ocean analysis and forecasting systems. Observing System Experiments (OSEs) are a classical tool for evaluating the impact and importance of an observing system on a data assimilation system. OSEs involve the systematic withholding of a sub-set of observations. The evaluation of the degradation in quality of the resulting analyses and forecasts is then used to quantify the impact of the observations withheld.

In the last decade, several studies based on OSEs have analyzed the impact of different components of the global ocean observing system for ocean analysis and forecasting. Balmaseda et al. (2007) studied the statistical impact of Argo on analyses of the global ocean for the period 2001–2006. Oke and Schiller (2007) analyzed the importance of the combination of Argo, Sea Surface Temperature (SST) and altimeter data on a regional eddy-resolving ocean reanalysis. Other relevant studies (e.g. Vidard, 2007; Tranchant, 2008; Guinehut, 2012 or more recently Fujii, 2015 and Lea et al., 2014) have focused on different observing systems and assessed

OSD
12, 1145–1186, 2015

their impact on analyses and forecasting systems. The GODAE OceanView program (https://www.godae-oceanview.org/), created to promote and coordinate operational oceanography worldwide, has set up a specific OSE task team (OSEval-TT) to formulate requirements for the enhancement of the global ocean observing system. More recently, the Tropical Pacific Observing System 2020 GOOS project (OOPC, 2014) has identified the importance of OSEs for assessing the role of the Tropical Pacific Observing system from a data assimilation perspective.

In this paper, we focus on the Argo observing system and its impact on the analyzed temperature (T) and salinity (S) structure of the ocean. Several OSEs are performed to assess the importance of Argo T and S profiles with the real-time Mercator global $1/4^{\circ}$ operational data assimilation system. The paper is organized as follows: the real time analysis and forecasting system and the experimental strategy are described in Sect. 2. Section 3 details the results and the conclusion is given in Sect. 4.

2 Tools and methods

2.1 Data assimilation system

The Mercator-Ocean $1/4^{\circ}$ operational global ocean analysis and forecasting system (Lellouche et al., 2013) (hereafter referred to as PSY3) was used for this study. The PSY3 system has been operational since 2005. It routinely assimilates Sea Level Altimetry (SLA), satellite Sea Surface Temperature (SST) and in situ data from Argo profiling floats, XBT, moorings (TAO-TRITON/PIRATA), gliders and also Conductivity, Temperature, and Depth probes (CTDs) from oceanographic vessels. The model is Version 3.1 of NEMO (Madec and the NEMO team, 2008) with a $1/4^{\circ}$ tri-polar ORCA grid. The horizontal resolution is 27 km at the Equator and decreases to 6 km toward the poles. 50 vertical levels are used and discretization decreases from 1 m resolution at the surface down to 450 m at the bottom, with 22 levels within the upper 100 m. The NEMO system uses the OPA Ocean model coupled with the LIM2 ice model (Fichefet

OSD
12, 1145–1186, 2015

and Morales Maqueda, 1997). Three-hour atmospheric fields from the European Centre of Medium Weather Forecasting (ECMWF) are used to force the ocean and ice models. Momentum and sea surface fluxes are computed from CORE bulk formulae (Large and Yeager, 2009). The data assimilation scheme was developed at Mercator-Ocean (Tranchant at al., 2008; Lellouche et al., 2013). It is based on a reduced-order (singular evolutive extended) Kalman filter (SEEK) (Pham et al., 1998) with localized 3-D multivariate modal decomposition of the forecast error and a 7 day assimilation window. A 3-D-Var scheme provides a correction of the slowly evolving large-scale biases in temperature and salinity below the mixed layer. The calculated increments are applied progressively using an Incremental Analysis Update (IAU) method.

The 2012 assimilated observation data sets include along-track altimeter SLA data from SSALTO/DUACS (Dibarboure et al., 2012). Mean Dynamic Topography (MDT), used as a reference for SLA data assimilation, is based on the "CNES-CLS09" MDT derived from observations and described in Rio et al. (2011). It was modified using a global $1/4^{\circ}$ reanalysis MDT (Greiner, personal communication). The assimilated SST observations are the NCDC/NOAA daily high-resolution SST analysis at $1/4^{\circ}$ resolution (Reynolds et al., 2007). In-situ temperature and salinity profiles from the Coriolis data center are also assimilated. Table 1 summarizes PSY3 characteristics.

The altimeter products were produced by Ssalto/Duacs and distributed by Aviso with support from CNES (http://www.aviso.altimetry.fr/). MDT_CNES-CLS09 was produced by CLS Space Oceanography Division and distributed by Aviso, with support from CNES (http://www.aviso.altimetry.fr/).

2.2 In-situ observations

The 2012 in situ dataset is extracted from the Coriolis data base (Cabanes et al., 2013). Coriolis is the in situ component of the French operational oceanography infrastructure. It provides real-time and qualified ocean in situ measurements to the European My-Ocean project (Copernicus Marine Service) and to research and climate communities. Coriolis collects, controls and standardizes temperature and salinity profiles from differ-

OSD
12, 1145–1186, 2015

ent types of instrument including Argo floats, CTDs from research vessels, expendable bathythermographs (XBTs), moorings, sea mammals, gliders and drifting buoys. Argo is currently by far the most important source of information for in situ temperature and salinity profiles.

Argo floats provide measurements of temperature and salinity from the surface to 2000 m every 10 days at the global scale. There were more than 3000 floats drifting over the global ocean in 2012, with less than 3° mean spacing. The XBT network provides temperature measurements mostly along the main shipping routes from the surface to a depth of 800 m. Moorings are mostly in the tropical oceans with TAO/TRITON moorings for the Pacific, PIRATA for the Atlantic and RAMA for the Indian Ocean. Typically the buoys sample the ocean from the surface down to 500 or 750 m with 10 to 15 levels. Other moorings sample specific regions such as the Drake Passage or the Labrador Sea. CTDs carried by sea mammals are located in high-latitude regions such as the Svalbard Islands, the French Southern and Antarctic Lands and the Ross Sea. Gliders are used to sample temperature and salinity from the surface to a given parking depth in specific areas of interest. There is not yet a global measurement strategy for such an observing system.

The 2012 coverage of the in situ dataset is shown in Fig. 1. Figure 1a and b each correspond to 50 % of the Argo datasets. To ensure that all Argo profiles were selected, we sorted data from the instrument type variable, *WMO_INST_TYPE*, specified as "*VERTICAL PROFILING: observation*" for Argo floats in the Coriolis dataset. The most realistic way of dividing up the Argo dataset and of keeping coherent spatial and temporal resolution was therefore to sort it by platform numbers. Odd-numbered Argo platforms are shown in Fig. 1a, even ones in Fig. 1b. One of the most striking features of these two plots is the global and dense coverage of the oceans. The sparse distribution of the No Argo dataset (green dots) is also remarkable. Some regions are rather more densely sampled by No Argo platforms than others. Figure 2 represents the time coverage of temperature (Fig. 2a) and salinity (Fig. 2b) profiles from the surface down

OSD
12, 1145–1186, 2015

to 2000 m for the last 6 months of 2012. The time distribution is fairly regular and no specific feature should impact our conclusions.

2.3 Experiment design

The OSEs presented here focus on the impact of the Argo observing system on temperature and salinity analyses and forecasts. Three experiments were performed from 18 January 2012 to 26 December 2012. This corresponds to 50 analyses with an assimilation cycle of 7 days. The three experiments assimilate SLA and SST data and differ only as regards the in situ assimilated data sets:

- The experiment entitled Run-Ref assimilates SLA, SST and all in situ data (Argo + "Other No Argo in situ data").
- The experiment entitled Run-Argo2 assimilates SLA, SST, 50 % of the Argo data and all the "other No Argo in situ data".
- The experiment entitled Run-NoArgo assimilates SLA, SST and all "other No Argo in situ data".

For the above three experiments, the strategy is to start from the same initial conditions from the PSY3 operational system that assimilates all the data and then withdraw part of the Argo dataset for the OSEs. Lastly, a free run (i.e. where no data at all are assimilated), hereafter called Free-Run, was also carried out to assess the overall improvement of the PSY3 system. The free run starts from the same initial conditions as for the three above-mentioned experiments. Table 2 summarizes the experiment strategy.

3 Results

This section is organized as follows. The first part is an independent comparison of the Run-NoArgo analyzed fields with Argo observations. This is the easiest way to assess

OSD
12, 1145–1186, 2015

the impact of Argo on the system. The second part compares analyzed temperature and salinity fields from the different OSEs. This quantifies the amplitude and the spatial distribution of the impact of Argo data assimilation. We then verify that changes observed in the analyzed fields also correspond to a decrease of the misfit with (assimilated) in situ observations. The last part compares Argo observations with co-located profiles from forecasted fields. This enables us to quantify the forecasting assimilation skills of our system. In each sub-section, temperature and salinity results are discussed separately.

3.1 Comparison of Run-NoArgo assimilated fields with Argo observations

Figure 3 shows the spatial distribution of the mean and RMS of the temperature difference between Argo observations and the Run-NoArgo analysis. RMS and mean statistics are calculated in $2^{\circ} \times 2^{\circ}$ boxes and in the 0–300 and 700–2000 m layers. This method can be used to assess the performance of the PSY3 system when no Argo data are available. It is assessed with independent data, as Argo profiles were not assimilated.

Figure 3a shows that, in the 0–300 m layer, our model without Argo data assimilation fails to correctly represent temperature fields over large regions. As expected, errors are also larger in western boundary currents and in the thermocline in the tropics where a small misplacement leads to large temperature errors due to the sharpness of the thermocline. RMS of the differences between analyzed fields and Argo observations in these regions reaches 1.5 °C. Mid-latitude gyres in the Atlantic, Pacific and Indian Oceans have smaller errors. However, RMS in these regions is still around 0.75 °C. The mean of the differences between analyzed field and observations is calculated on a similar basis as the RMS. The mean of the temperature differences reveals that without Argo assimilation, western boundary currents are 0.5 °C warmer than observations. The tropical Pacific Ocean is cooler (−0.6 °C) than Argo observations in the western part.

OSD
12, 1145–1186, 2015

In the 700–2000 m layer, errors are more spatially concentrated. The RMS differences between Run-NoArgo analyzed fields and Argo observations in the western boundary currents is over 0.25 °C but can reach 0.4 °C in particular areas. The analyzed temperature of the regions between the Antarctic and Indian Oceans are also very different from Argo measurements. The North Atlantic and Arabian Sea show RMS temperature differences of 0.4 and 0.2 °C respectively. In the tropics, the RMS reaches 0.15 °C. In the middle of the Pacific sub-tropical basin, the contribution of Argo assimilation is less obvious from that point of view as the RMS in that part of the ocean is lower than 0.1 °C. The mean misfit does not reveal any significant bias in that layer in this region.

Figure 4 is similar to the previous figure but concerns salinity. Figure 4a shows the RMS differences between analyzed salinity and Argo observations in the 0–300 m layer. At that depth, mid-latitude oceans, North Indian Ocean, North Pacific, Atlantic, western boundary current regions and part of the Antarctic Ocean show differences larger than 0.1 PSU and could be considered as regions very sensitive to salinity observations, unlike South Pacific, South Indian Ocean and part of the Antarctic Ocean. The distribution of the mean salinity differences (Fig. 4c) shows particular patterns in the Antarctic Ocean between South Africa and Australia, in the East Indian Ocean and also in the South Atlantic Ocean. The analyzed ocean in these regions displays a stronger positive salt bias.

From 700 to 2000 m (Fig. 4b), the North Atlantic basin, outflow regions, western boundary current regions and part of the Antarctic Ocean between South Africa and Australia have large RMS misfits. In this layer, the mean salinity misfit is greatest in the Antarctic Ocean and Mediterranean outflow region (Fig. 4d). In this depth range, the analysis is likely to be sensitive to Argo assimilation as there are very few other in situ data to constrain it.

OSD
12, 1145–1186, 2015

3.2 Impact of Argo data assimilation on analyzed fields

In the next two sub-sections, we discuss the impact of the Argo dataset on temperature and salinity analyzed fields from the surface down to a depth of 2000 m. In each sub-section, we study a snapshot of the daily difference between OSEs with and without Argo data assimilation to illustrate the impact of Argo. We then use the spatial RMS of the daily differences in the 0–300 and 700–2000 m layers to provide quantitative information (geographical areas, amplitude) for determining the impact of Argo observations. Heat and salt content in the 0–2000, 0–300 and 700–2000 m layers are also analyzed. This shows the sensitivity of the analyzed temperature and salinity fields to Argo data assimilation. We then verify that the impact observed on analyzed fields when Argo data are assimilated also corresponds to a reduction of in situ observation-analysis differences (i.e. a reduction of misfits).

3.3 Temperature

Figure 5 shows the temperature differences between Run-Ref and Run-NoArgo for the 19 December 2012 at 100 and 1000 m. We chose that date to illustrate the accumulated state of the analyzed ocean at the end of a year-long experiment.

The impacts of Argo observations at 100 m (Fig. 5a) are widely but unequally distributed in the global ocean. Many regions show differences higher than 0.3 °C, mostly in the Northern Hemisphere and in the equatorial band. In some regions, these one-day differences reach 1 °C or more.

At 1000 m the influence of Argo observations is much more localized: analyses for North Atlantic Ocean, Agulhas current, south of Australia and south Indian Ocean are strongly affected by Argo assimilation. In these highly dynamic regions, differences between the two experiments reach 0.5 °C. The influence of Argo observations at 1000 m is striking in the North Atlantic area in the outflow from the Mediterranean; differences there can be larger than 0.3 °C. As a consequence, Argo data assimilation seems crucial to improve the model of water mass properties in the ocean interior.

OSD
12, 1145–1186, 2015

Figure 6 shows the RMS of the temperature differences between Run-Ref and Run-NoArgo. It is calculated from the daily differences of the last 6 months of experiment. It quantifies the spatial distribution of the impact of Argo assimilation on the PSY3 data assimilation system. We chose to focus on the 0–300 m layer, where SST and SLA assimilation also plays a major role, in order to evaluate the importance of Argo temperature measurements in the upper ocean, and on the 700–2000 m layer to assess the impact of Argo profiles in this specific layer, where Argo is almost the only in situ observing system available.

Figure 6a shows that global ocean analyses are impacted by assimilating the Argo data in the 0–300 m layer. The RMS of the temperature differences between experiments reaches 0.5 °C in each ocean. The highest values of the RMS (around 1.5 °C) are located in regions where the variability is very high (Gulf Stream, Kuroshio, Brazilian current, Agulhas current, North Brazil current retroflection). Argo assimilation in these regions strongly impacts analyzed temperature fields.

In the 700–2000 m layer, the impact of Argo on analyzed temperature fields is more localized in regions with high variability. In the Gulf Stream, the Agulhas current and around South Africa the RMS of the temperature differences reaches 0.5 °C. In this depth range, the North Atlantic remains the most sensitive region to Argo data assimilation. RMS of the temperature differences in the Red Sea and Mediterranean outflow region is around 0.5 °C. On the other hand, the impact of Argo in the 700–2000 m layer is not as widely dispersed as in the 0–300 m layer. The RMS remains significant (around 0.2 °C) in the South Atlantic, Indian Ocean and part of the Antarctic Ocean. Pacific Ocean analyses in that layer are less impacted by the assimilation of Argo data.

Figure 7 shows the spatial distribution of the mean and RMS of the temperature difference between Argo observations and the Run-Ref analysis which assimilates Argo observations together with satellite and other in situ observations. RMS and mean statistics are calculated in 2° × 2° boxes and in the 0–300 and 700–2000 m layers. Differences are obviously much reduced compared to the Run-NoArgo experiment (Fig. 3), which shows that the assimilation system is able to retain most of the information de-

OSD
12, 1145–1186, 2015

rived from Argo observations and there is no significant incompatibility with the other assimilated data sets (e.g. satellite altimetry). In what follows, Run-Ref will be considered as our best estimate of the real ocean and we will further quantify the impact of Argo observations by comparing Run-Argo2 and Run-NoArgo analyzed fields to Run-Ref fields.

Figure 8 is the time series of heat content anomaly estimates in different oceans and for different depth ranges. Heat content changes are calculated as described in von Schuckmann et al. (2009). Anomalies are obtained by subtracting the 3 year mean (2011–2013) of PSY3 analyzed fields from the OSEs analyzed temperature. Time series for the Global Ocean, North Atlantic Ocean (20–60° N; 5–70° W), North Pacific Ocean (20–60° N; 110° W–120° E) and Southern Oceans (50–70° S; 180° W–180° E) are shown in Fig. 8.

Global Ocean Heat Content (hereafter referred to as GOHC) anomaly is an important diagnostic measure of changes in the Earth's climate system (Levitus et al., 2005; Hansen et al., 2005). This diagnostic measure is often derived from Argo observations (e.g. von Schuckmann et al., 2011 and 2009; Willis et al., 2009; Trenberth and Fasullo, 2009) or other observing systems such as altimetry or through the closure of the Earth's Energy Budget (e.g. Domingues et al., 2008; Cazenave and Llovel, 2010; Trenberth, 2010).

Figure 8a shows an overestimation of the GOHC anomaly calculated without Argo observations that is significant compared to the variability of the system. In the 0–2000 m layer, GOHC anomaly difference between Run-Ref and Run-NoArgo is around $0.8 \times 10^8\,\mathrm{J\,m^{-2}}$. The anomaly for the three OSEs varies from -1×10^8 to $2 \times 10^8\,\mathrm{J\,m^{-2}}$. This difference is mainly driven by the estimation of the heat content anomaly in the 700–2000 m layer where the discrepancy between experiments reaches $0.4 \times 10^8\,\mathrm{J\,m^{-2}}$. In the 0–300 m layer, the differences between the OSEs are less significant.

Focusing on different ocean regions (Fig. 8b–d) shows that the impact of Argo differs depending on regions and hemispheres. In the North Atlantic Ocean, in the 700–

OSD
12, 1145–1186, 2015

2000 m layer, ocean analysis without Argo observation gives warmer results than our best ocean estimate. The Heat Content anomaly reaches 1.4×10^8 J m^{-2}, which is significant when compared to the heat content variability there. It is also noticeable that the impact is not necessarily in the same direction. Contrary to the North Atlantic Ocean and the South Oceans, Heat Content anomaly is reduced without Argo assimilation in the North Pacific Ocean. Moreover, the negative Heat Content anomaly leads to compensation between the Heat Content anomalies in different oceans that hide the importance of Argo observations in the GOHC evaluation.

These experiments show the high sensitivity of the OHC estimation from the PSY3 analysis to the assimilation of the Argo observation array. This is especially true for depths below 700 m, where the variability is smaller than in the surface layer. Estimates differ if only half of the Argo floats are assimilated.

3.3.1 Salinity

Figure 9 shows the salinity differences between Run-Ref and Run-NoArgo for the 19 December 2012 at 100 and 1000 m. At 100 m, significant differences are spread all over the global ocean. Many regions are heavily affected by Argo assimilation, such as the tropical oceans and the Gulf Stream area. Around the equator, the maximum amplitude of the daily differences is larger than 0.3 PSU. The spread and amplitude of differences show the sensitivity of the PSY3 analysis to the assimilation of Argo salinity data.

At 1000 m, North Atlantic regions are very sensitive to the assimilation of Argo profiles, because the differences reach 0.1 PSU. The impact is greatest in the Mediterranean and Red Sea outflows and the Gulf Stream areas. Regions with high variability are also significantly impacted: western boundary current, South Indian Ocean, Antarctic Circumpolar Current (ACC) and Arabian Sea. There is no significant difference in the Pacific and South Atlantic Oceans at that depth for this date.

Figure 10 shows the RMS of the salinity differences between Run-Ref and Run-NoArgo. Similar results are obtained for salinity and temperature. In the 0–300 m layer,

OSD
12, 1145–1186, 2015

the impact of the assimilation of Argo salinity profiles is spread over all of the world's oceans. RMS of the salinity difference between OSEs reaches 0.1 PSU in most of the oceans. Tropical oceans and western boundary current regions are the most affected; RMS exceeds 0.2 PSU in these areas. The tropical Atlantic is the most sensitive region. The Amazon outflow is extremely active and the sensitivity of the analyses to the assimilation of Argo profiles is clear to see.

It is also noticeable that the Labrador Sea, mainly along its shelf break, is also very sensitive to Argo profile assimilation. The analyses for the "boundary" between the Indian Ocean and the Antarctic, where the subtropical front approaches the Agulhas front, are also highly affected. The analysis of these different water masses is obviously very sensitive to Argo salinity and temperature profile assimilation.

In the 700–2000 m layer, the greatest impact is found in the North Atlantic Ocean. RMS of the salinity differences reaches 0.1 PSU along the European coast and is around 0.05 PSU elsewhere in the basin. As for temperature, high-variability regions are strongly affected by Argo profile assimilation: Arabian Sea, Agulhas current region, South America west boundary region and southern Indian Ocean. Again, the Pacific Ocean is far less affected.

Figure 11 shows the spatial distribution of the mean and RMS of the salinity difference between Argo observations and the Run-Ref analysis which assimilates Argo observations together with satellite and other in situ observations. RMS and mean statistics are calculated in $2^{\circ} \times 2^{\circ}$ boxes and in the 0–300 and 700–2000 m layers. This shows that the system performs best when all Argo floats are assimilated. Compared to Fig. 4a–d where no Argo data were assimilated, the misfit with in situ observation is considerably reduced. Results are similar for salinity and temperature. For salinity also, Run-Ref will be considered as our best salinity estimate of the real ocean and we will also further quantify the impact of Argo observations by comparing Run-Argo2 and Run-NoArgo analyzed salinity fields to Run-Ref ones.

Figure 12 shows the evolution of the daily salt content anomaly in different regions of the global ocean and for different layers. The salt content anomaly is calculated by

OSD
12, 1145–1186, 2015

subtracting the 3 year mean (2011–2013) of the operational PSY3 system salinity from the OSEs analyzed salinity. Time series for the Global Ocean, North Atlantic Ocean (20–60° N; 5–70° W), North Pacific Ocean (20–60° N; 110° W–120° E) and Southern Oceans (50-70° S; 180° W–180° E) are plotted. The different OSEs are represented by different colors. Blue is for Run-Ref, light blue is for Run-Argo2 and black is for Run-NoArgo.

The global estimate of the salt anomaly (Fig. 12a) shows differences depending on whether it is calculated with the Run-Ref, Run-Argo2 or Run-NoArgo. This masks some larger differences in regional estimates. Even the salt anomaly estimate in the surface layers from 0 to 300 m shows a strong sensitivity to the assimilation of Argo profile data, especially in the Southern Ocean region. At depths of between 700 and 2000 m, where Argo is nearly the only in situ observing system available, the impact on the estimated variability of the salt anomaly is significant compared to the natural variability, even on one-year experiments. The results for the North Atlantic Ocean are the most heavily affected. The contribution of the 700–2000 m layer to the 0–2000 m salt anomaly is not negligible.

In most of the regions, salt content estimation differs whether only half or the full Argo array is assimilated. The estimates obtained with half of the Argo array are, in most cases, closer to the estimate obtained with the full Argo array than the simulation without Argo, but the differences are still significant compared to the anomaly itself.

3.4 Impact on forecast fields

In this section, the impact of Argo data assimilation on short term forecasts (< 7 days) is evaluated using the innovation (observation values minus model forecast values) statistics. OSEs forecast fields are compared with as yet non-assimilated Argo and other in situ observations.

OSD
12, 1145–1186, 2015

3.4.1 Temperature innovations

Figure 13 shows the global average RMS of the temperature innovation from 0 to 2000 m for the last 6 months of the Run-Ref, Run-Argo2, Run-NoArgo and Free Run experiments.

For each experiment, the RMS is greatest at approximately 100 m and decreases with depth. The amplitude of the RMS temperature innovations below 1000 m is very low compared to the mixed layer depth values but global variability at that depth is obviously also very low. The RMS of temperature innovation decreases the greater the quantity of Argo data assimilated. Atmospheric forcing and assimilation of SST and SLA may explain the good surface results for Run-Ref, Run-Argo2 and Run-NoArgo.

Figure 14a shows the temporal mean RMS temperature innovation profile of the previous 6 month time series from the surface down to 2000 m. This is a standard procedure for characterizing the performance of a forecasting system and evaluating the impact of an observing system (Oke and Schiller, 2007; Vidard et al., 2007; Fujii et al., 2015; Lea et al., 2014; Guinehut et al., 2012). Maximum RMS is found at 100 m for the 4 experiments, but RMS of innovations range from 1.4 °C for Free Run to 0.9 °C for Run-Ref. The RMS of temperature innovations is improved in the whole water column when Argo temperature profiles are assimilated. However, at depths greater than 1400 m, the RMS for temperature innovation of the Free Run experiment is lower than temperature innovation RMS for the Run-NoArgo. This result shows the importance of Argo T and S profile assimilation for ensuring a good projection at depth of the SLA and SST innovation by the multivariate data assimilation system.

On Fig. 14b, each RMS temperature innovation profile shown on Fig. 14a is normalized with the Run-Ref RMS innovation profile, which represents our best forecast, in blue on Fig. 14a and b. We can then quantify the degradation of system performance in terms of temperature RMS error forecast due to the decrease of the number of Argo profiles assimilated. From those normalized profiles, we deduce an estimation of the percentage of degradation of the system performance for different depth ranges, sum-

OSD
12, 1145–1186, 2015

marized in Table 3. Coarsely, improvements range from 10 % in the 0–300 m layer to 50 % in the 700–2000 m layer. Assimilation of the first half of the Argo array improves the performance of the system by 15 % from the surface to 300 m depth and from 15 to 30 % in the 700–2000 m layer. The assimilation of the second part of the array improves the performance of the system by around 5 % in the 0–300 m depth and by 10 to 20 % in the 700–2000 m layer.

3.4.2 Salinity innovation

The same calculations are performed for salinity as for temperature. Figure 15 is a time series of the RMS of salinity profile innovations for the last 6 months of experiments. Run-Ref, Run-Argo2, Run-NoArgo and Free Run time series are represented here.

The RMS error is greatest at the surface and decreases with depth. From 0 to 2000 m the more salinity data are assimilated the closer to the observation the forecasts become. There is no significant increase of the innovation RMS during the 6 month experiment for Run-Ref and Run Argo2 as there is in Run-NoArgo and Free Run. This increase becomes visible at around 300 m. This result demonstrates the importance of Argo observations for constraining salinity in the PSY3 system.

Figure 16 shows the global mean absolute and normalized profiles of the RMS of salinity innovations for the different experiments. In the 0–300 m layer, the RMS innovation improvement depends on the quantity of Argo data assimilated by the system. Figure 16b shows that the RMS of the innovations is reduced by 20 % when the first half of Argo profiles is assimilated compared the RMS without Argo data assimilated. The assimilation of the second half of the Argo data set reduces it by a further 5 to 10 % relative to the best scores (Run-Ref in blue). In the 700–2000 m layer, the increase of the quantity of Argo data assimilated, together with SLA and SST, induces a decrease of the RMS misfit in salinity. The Free Run results are closer to salinity observations than the Run-NoArgo results at depth. This was also found for the temperature innovation. This again shows the need for a good coverage of in situ profiles to estimate a coherent T and S 3-D-correction from data assimilation of SLA and SST.

OSD
12, 1145–1186, 2015

The improvement corresponding to the assimilation of 50 % of the Argo array is from 20 to 40 % in that layer, compared to Run-NoArgo. Assimilation of the second half of the Argo array reduces the RMS innovation by a further 10 to 25 % compared to the best results. These values are recapitulated in Table 4.

4 Conclusion

Observing System Experiments were carried out with the real time Mercator-Ocean 1/4° global ocean system to quantify the impact of Argo data assimilation. We considered the effect of Argo data assimilation on the 0–2000 m layer, focusing on the 0–300 m layer and on the 700–2000 m layer, where Argo observations are almost the only in situ observing system. The different OSEs cover the year 2012.

The quality of the analyses without Argo observations was first assessed using independent non-assimilated Argo data. This highlighted the system's weaknesses when only SST, SLA and non-Argo in situ data are assimilated. Without Argo data assimilated, large errors are found in the western boundary currents, ACC, Mediterranean and Red Sea outflows and in the tropics.

The impact of Argo data assimilation was then assessed through the comparison of the analyzed temperature and salinity fields over the last 6 months from the different experiments. The comparison of the Run-Ref and Run-NoArgo experiments highlights the high sensitivity of the analyses to Argo data assimilation. The 6 month RMS differences of daily fields between these experiments easily reach 1 °C and 0.1 PSU at 100 m and 0.3 °C and 0.05 PSU at 1000 m. The location of the main discrepancies is strongly correlated to regions with high variability, both at the surface and at depth. Strong effects are also noted in the Red Sea, Amazon and Mediterranean outflow regions. Regions sensitive to Argo data assimilation coincide well with the regions where there is a large difference between analyzed fields without Argo observations and in situ observations.

OSD
12, 1145–1186, 2015

The changes over time to integrated values such as heat content anomaly or mean salinity anomaly from different regions and depths shows that Argo data assimilation has a considerable impact on the estimated evolution of heat content and mean salinity anomaly in both the surface layer from 0 to 300 m and the 700–2000 m layer, the latter being mainly unobserved without Argo observations.

Finally, we evaluate the skill of the PSY3 forecasting system by computing the RMS differences between in situ observations and forecast fields for the different OSEs. Through Argo assimilation the differences between observation and forecast fields are reduced by about 20 % in the 0–300 m layer and by between 20 and 65 % in the 700–2000 m layer. Results at depth show the importance of the global spatial coverage of Argo assimilation for constraining the temperature and salinity 3-D-correction deduced from data assimilation of SLA and SST, for more realistic results.

We show that the impact noted in the analyzed PSY3 temperature and salinity fields when Argo is assimilated corresponds to an improvement of the analysis and forecast fields in terms of innovation and residuals to in situ observations. This shows the ability of the data assimilation system to take advantage of the Argo observations. The progressive improvement of the system skills from assimilation of half of the Argo array to the full Argo array also indicates that all observations are needed to constrain our system. These results highlight the major importance of Argo data assimilation for operational oceanography. A decrease in the existing coverage of the Argo array would lead to a degradation of the PSY3 global ocean analysis and forecasts.

Finally, it is important to bear in mind that results from OSEs depend on the modeling and data assimilation system used. General statements about observing systems should only be made with caution unless consistent results based on several systems are obtained. This is the approach promoted by the GODAE OceanView OSE/OSSE task team. As our results are consistent with and complement those carried out by other teams (e.g. Lea et al., 2014), we believe that our statements on the major contribution of Argo to global ocean analysis and forecasting systems are robust and can be generalized to include other systems.

OSD
12, 1145–1186, 2015

Acknowledgements. The research leading these results has received funding from the European FP7 program under the E-AIMS project. The authors would like to thank Jean-Michel Lellouche and Olivier Le Galloudec for providing support on the use of the operational system, Charly Régnier for providing the diagnostic tools and Gilles Garric and Yann Drillet for comments on an earlier version of the manuscript.

References

Balmaseda, M., Anderson, D., and Vidard, A.: Impact of Argo on analyses of the global ocean, Geophys. Res. Lett., 34, L16605, doi:10.1029/2007GL030452, 2007.

Bell, M. J., Lefebvre, M., Le Traon, P.-Y., Smith, N., and Wilmer-Becker, K.: GODAE: The global ocean data assimilation experiment, Oceanography, 22, 14–21, doi:10.5670/oceanog.2009.62, 2009.

Benkiran, M. and Greiner, E.: Impact of the incremental analysis updates on a real-time system of the North Atlantic Ocean, J. Atmos. Ocean. Technol., 25, 2055–2073, 2008.

Boyer, T., Levitus, S., Antonov, J., Locarnini, R., Mishonov, A., Garcia, H., and Josey, S. A.: Changes in freshwater content in the North Atlantic Ocean 1955–2006, Geophys. Res. Lett., 34, L16603, doi:10.1029/2007GL030126, 2007.

Cabanes, C., Grouazel, A., von Schuckmann, K., Hamon, M., Turpin, V., Coatanoan, C., Paris, F., Guinehut, S., Boone, C., Ferry, N., de Boyer Montégut, C., Carval, T., Reverdin, G., Pouliquen, S., and Le Traon, P.-Y.: The CORA dataset: validation and diagnostics of in situ ocean temperature and salinity measurements, Ocean Sci., 9, 1–18, doi:10.5194/os-9-1-2013, 2013.

Cazenave, A. and Llovel, W.: Contemporary sea level rise, Annu. Rev. Mar. Sci., 2, 145–173, 2010.

Dibarboure, G., Pujol, M.-I., Briol, F., Le Traon, P.-Y., Larnicol, G., Picot, N., Mertz, F., and Ablain, M.: Jason-2 in DUACS: first tandem results and impact on processing and products, Mar. Geod., 34, 214–241, doi:10.1080/01490419.2011.584826, 2011.

Domingues, C. M., Church, J. A., White, N. J., Glecker, P. J., Wijffels, S. E., Barker, P. M., and Dunn, J. R.: Improved estimates of upper-ocean warming and multi-decadal sea-level rise, Nature, 453, 1090–1094, doi:10.1038/nature07080, 2008.

OSD
12, 1145–1186, 2015

Fichefet, T. and Morales Maqueda, M. A.: Sensitivity of a global sea ice model to the treatment of ice thermodynamics and dynamics. J. Geophys. Res., 102, 12609–12646, doi:10.1029/97JC00480, 1997.

Fujii, Y., Cummings, J., Xue, Y., Schiller, A., Lee, T., Balmaseda, A. M., Remy, E., Masuda, S., Alves, O., Brassington, G., Cornuelle, B., Martin, M. J., Oke, P. R., Smith, G., and Yang, X.: Evaluation of the Tropical Pacific Observing System from the Ocean Data Assimilation Perspective, Q. J. Roy. Meteor., accepted, 2015.

Guinehut, S., Dhomps, A.-L., Larnicol, G., and Le Traon, P.-Y.: High resolution 3-D temperature and salinity fields derived from in situ and satellite observations, Ocean Sci., 8, 845–857, doi:10.5194/os-8-845-2012, 2012.

Hansen, J., Nazarenko, L., Ruedy, R., Sato, M., Willis, J., Del Genio, A., Koch, D., Lacis, A., Lo, K., Menon, S., Novakov, T., Perlwitz, J., Russell, G., Schmidt, G. A., and Taunsnev, N.: Earth's energy imbalance: confirmation and implications, Science, 308, 1431–1435, doi:10.1126/science.1110252, 2005.

Large, W. G. and Yeager, S. G.: The Global Climatology of an inter-annually varying air–sea flux data set, Clim. Dynam., 33, 341–364, doi:10.1007/s00382-008-0441-3, 2009.

Lea, D., Martin, M. J., and Oke, P. R.: Demonstrating the complementarity of observations in an operational ocean forecasting system, Q. J. Roy. Meteor. Soc., 140, 2037–2049, doi:10.1002/qj.2281, 2014.

Lellouche, J.-M., Le Galloudec, O., Drévillon, M., Régnier, C., Greiner, E., Garric, G., Ferry, N., Desportes, C., Testut, C.-E., Bricaud, C., Bourdallé-Badie, R., Tranchant, B., Benkiran, M., Drillet, Y., Daudin, A., and De Nicola, C.: Evaluation of global monitoring and forecasting systems at Mercator Océan, Ocean Sci., 9, 57–81, doi:10.5194/os-9-57-2013, 2013.

Levitus, S., Antonov, J., and Boyer, T.: Warming the world ocean, 1955–2003, Geophys. Res. Lett., 32, L02604, doi:10.1029/2004GL021592, 2005.

Lindstrom, E., Gunn, J., Fischer, A., McCurdy, A., and Glover, L. K.: A Framework for Ocean Observing. By the Task Team for an Integrated Framework for Sustained Ocean Observing, UNESCO 2012, IOC.INF-1284, doi:10.5270/OceanObs09-FOO, 2012.

Oke, P. R. and Schiller, A.: Impact of Argo, SST, and altimeter data on an eddy-resolving ocean reanalysis, Geophys. Res. Lett., 34, L19601, doi:10.1029/2007GL031549, 2007.

OOPC: Report of the Tropical Pacific Observing System 2020 Workshop (TPOS2020), White Paper – Vol. II, available at: http://www.iode.org/index.php?option=com_oe&task=viewDocumentRecord&docID=13163, 2014.

OSD
12, 1145–1186, 2015

Pham, D. T., Verron, J., and Roubaud, M. C.: A singular evolutive extended Kalman filter for data assimilation in oceanography, J. Marine Syst., 16, 323–340, 1998.
Reynolds, R. W., Smith, T. M., Liu, C., Chelton, D. B., Casey, K. S., and Schlax, M. G.: Daily high-resolution blended analyses for sea surface temperature, J. Climate, 20, 5473–5496, 2007.
Rio, M. H., Guinehut, S., and Larnicol, G.: New CNES-CLS09 global mean dynamic topography computed from the combination of GRACE data, altimetry and in situ measurements, J. Geophys. Res., 116, C07018, doi:10.1029/2010JC006505, 2011.
Tranchant, B., Testut, C.-E., Renault, L., Ferry, N., Birol, F., and Brasseur, P.: Expected impact of the future SMOS and Aquarius Ocean surface salinity missions in the Mercator Ocean operational systems: new perspectives to monitor ocean circulation, Remote Sens. Environ., 112, 1476–1487, doi:10.1016/j.rse.2007.06.023, 2008.
Trenberth, K. E. and Fasullo, J. T.: The Ocean is warming, isn't it?, Nature, 465, 304, 2010.
Vidard, A., Anderson, D. L. T., and Balmaseda, M.: Impact of ocean observation systems on ocean analysis and seasonal forecasts, Mon. Weather Rev., 135, 409–429, doi:10.1175/MWR3310.1, 2007.
von Schuckmann, K., Gaillard, F., and Le Traon, P.-Y.: Global hydrographic variability patterns during 2003–2008, J. Geophys. Res., 114, 1–17, doi:10.1029/2008JC005237, 2009.
von Schuckmann, K. and Le Traon, P.-Y.: How well can we derive Global Ocean Indicators from Argo data?, Ocean Sci., 7, 783–791, doi:10.5194/os-7-783-2011, 2011.
Willis, J. K., Lymann, J. M., Johnson, G. C., and Gilson, J.: In-situ data biases and recent heat content variability, J. Atmos. Ocean. Technol., 26, 846–852, 2009.

OSD
12, 1145–1186, 2015

Table 1. Characteristics of the Mercator-Ocean PSY3 data assimilation system.

System Name	Resolution	Model	Assimilation	Assimilated observations
PSY3	Horizontal: 1/4° Vertical: 50 levels	ORCA025, NEMO 3.1, LIM2 EVP, Bulk CORE, 3 h atmospheric forcing (ECMWF)	SAM IAU 3-D-Var bias correction	Satellite "AVHRR" SST Altimeter SLA (+MDT) T/S vertical profiles

OSD
12, 1145–1186, 2015

Table 2. List of OSEs carried out as part of this study.

	SST	Altimeter SLA	Argo	Other in situ
Run-Ref	×	×	×	×
Run-Argo2	×	×	50 % of the array	×
Run-NoArgo	×	×		×
Free-Run				

OSD
12, 1145–1186, 2015

Table 3. Temperature forecast skill improvement derived from the reduction of the RMS temperature innovations.

	Forecast skill improvement due to assimilation of the first half of the Argo array	Forecast skill improvement due to assimilation of the global Argo array
0–2000 m	From 10 to 30 %	From 15 to 50 %
0–300 m	From 10 to 15 %	Around 18 %
700–2000 m	From 10 to 30 %	From 20 to 50 %

OSD
12, 1145–1186, 2015

Table 4. Salinity forecast skill improvement derived from the reduction of the RMS salinity innovations.

	Forecast skill improvement due to assimilation of the first half of the Argo array	Forecast skill improvement due to assimilation of the global Argo array
0–2000 m	From 20 to 40 %	From 20 to 65 %
0–300 m	Around 20 %	From 20 to 30 %
700–2000 m	From 20 to 40 %	From 30 to 65 %

OSD
12, 1145–1186, 2015

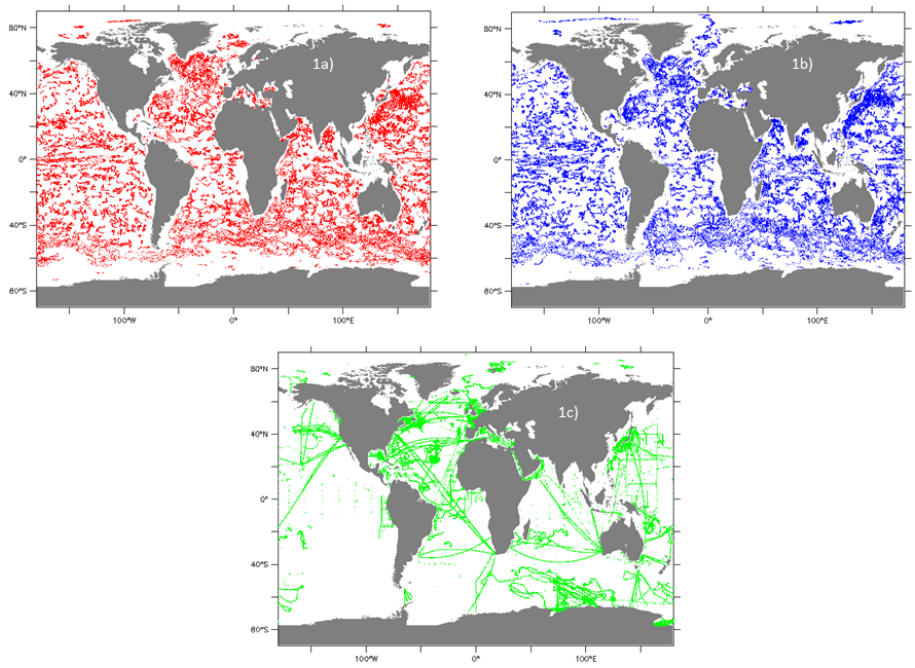

Figure 1. Spatial distribution of 2012 in situ dataset divided into 3 sub-datasets. Red dots are the odd Argo profiles, blue dots are even Argo profiles, green dots are the other in situ observations.

OSD
12, 1145–1186, 2015

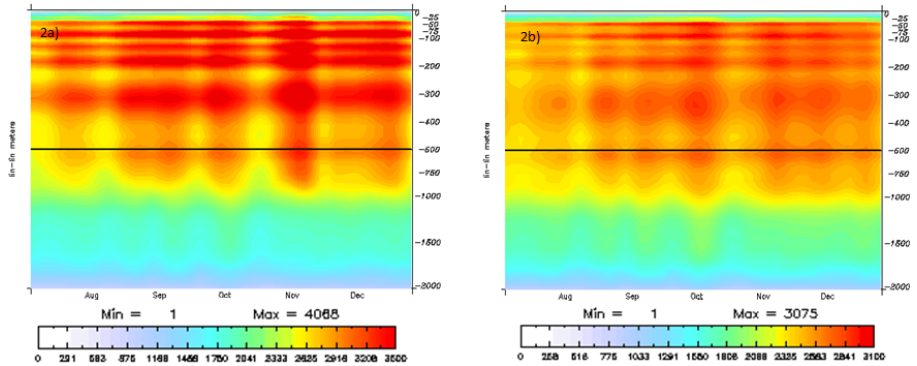

Figure 2. Time series of the number of 2012 in situ temperature **(a)** and salinity **(b)** data items from the surface to 2000 m per week.

OSD
12, 1145–1186, 2015

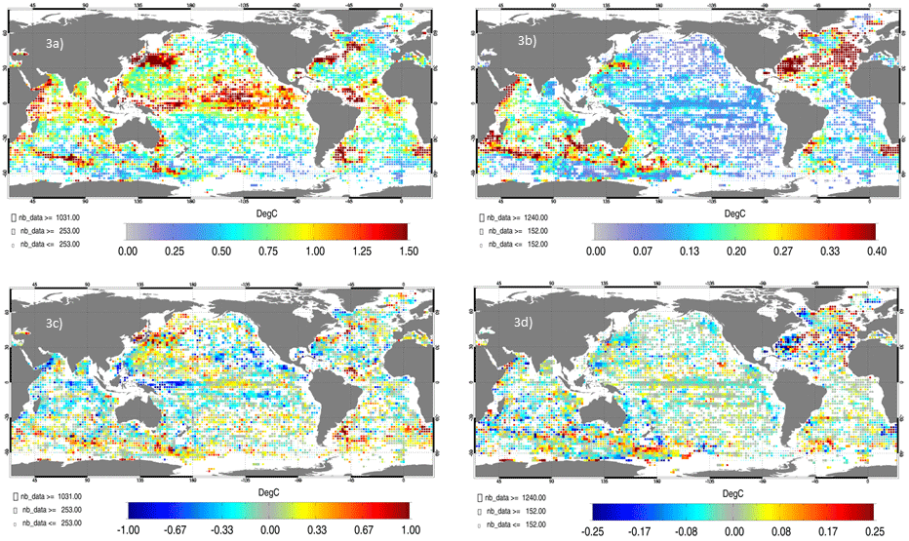

Figure 3. Spatial distribution of the RMS and the mean temperature differences between Run-NoArgo and Argo observations in the 0–300 and 700–2000 m layers: **(a)** shows the RMS temperature differences in the 0–300 m layer. **(b)** shows the RMS temperature differences in the 700–2000 m layer. **(c)** shows the mean temperature differences in the 0–300 m layer. **(d)** shows the mean temperature differences in the 700–2000 m layer.

OSD
12, 1145–1186, 2015

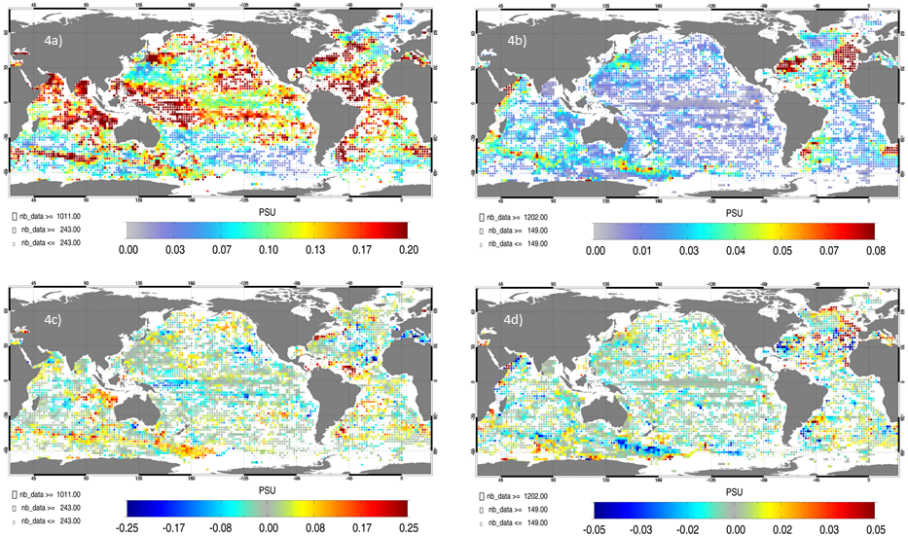

Figure 4. Spatial distribution of the mean and RMS salinity differences between Run-NoArgo and Argo observations in the 0–300 and 700–2000 m layers: **(a)** shows the RMS salinity differences in the 0–300 m layer. **(b)** shows the RMS salinity differences in the 700–2000 m layer. **(c)** shows the mean salinity differences in the 0–300 m layer. **(d)** shows the mean salinity differences in the 700–2000 m layer.

OSD
12, 1145–1186, 2015

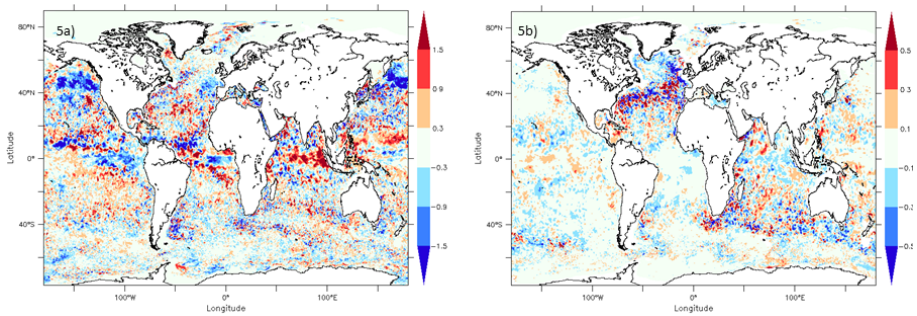

Figure 5. 19 December 2012: temperature analyzed fields – differences between Run-Ref and Run-NoArgo at 100 m **(a)** and 1000 m **(b)**.

OSD
12, 1145–1186, 2015

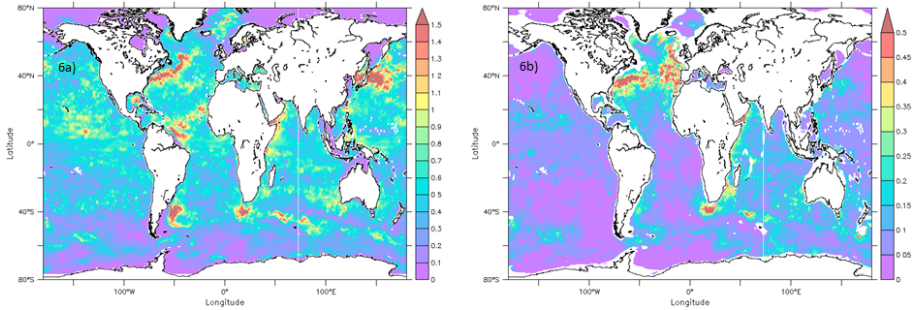

Figure 6. RMS of temperature differences between Run-Ref and Run-NoArgo in the 0–300 m layer **(a)** and in the 700–2000 m **(b)** layer for the last 6 months of the experiments.

OSD
12, 1145–1186, 2015

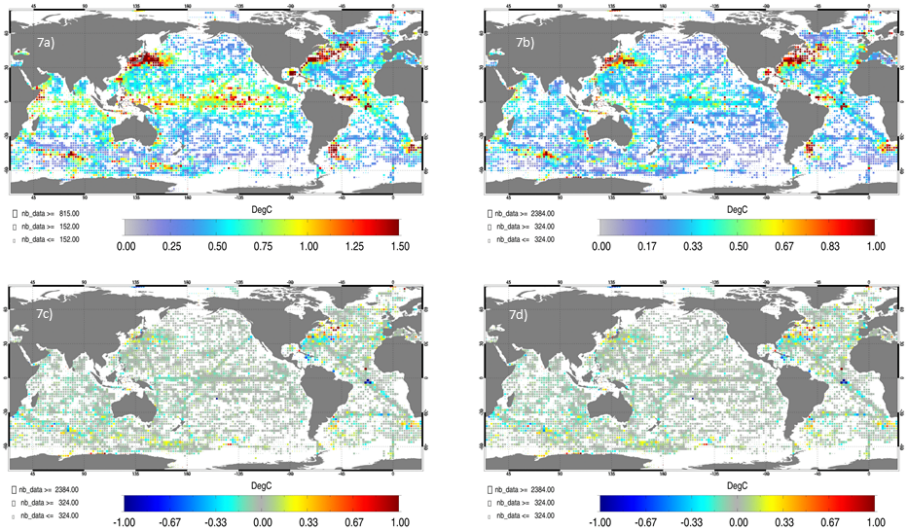

Figure 7. Spatial distribution of the mean and RMS temperature differences between Run-Ref and in situ observations in the 0–300 and 700–2000 m layers: **(a)** shows the RMS temperature differences in the 0–300 m layer. **(b)** shows the RMS temperature differences in the 700–2000 m layer. **(c)** shows the mean temperature differences in the 0–300 m layer. **(d)** shows the mean temperature differences in the 700–2000 m layer.

OSD
12, 1145–1186, 2015

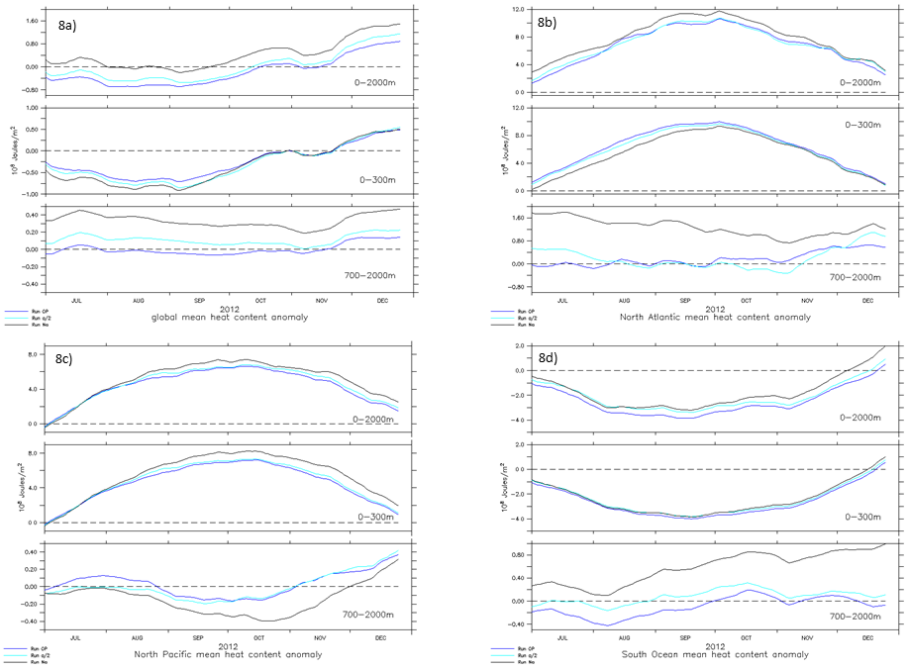

Figure 8. Heat content anomaly time series for 0–2000 m layer, 0–300 m layer and 700–2000 m layer for the Run-Ref (blue), Run-Argo2 (light blue) and Run-NoArgo (black) and for the Global Ocean **(a)**, North Atlantic Ocean **(b)**, North Pacific Ocean **(c)** and South Ocean **(d)**.

OSD
12, 1145–1186, 2015

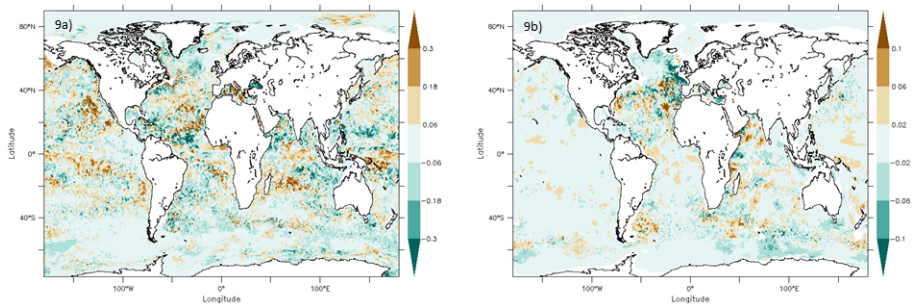

Figure 9. 19 December 2012, salinity analyzed fields – differences between Run-Ref and Run-NoArgo at 100 m **(a)** and 1000 m **(b)**.

OSD
12, 1145–1186, 2015

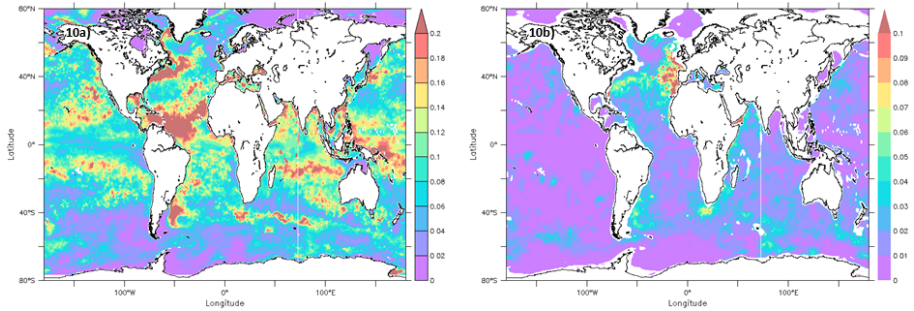

Figure 10. RMS of salinity differences between Run-Ref and Run-NoArgo in the 0–300 and 700–2000 m layers for the last 6 months of experiment.

OSD
12, 1145–1186, 2015

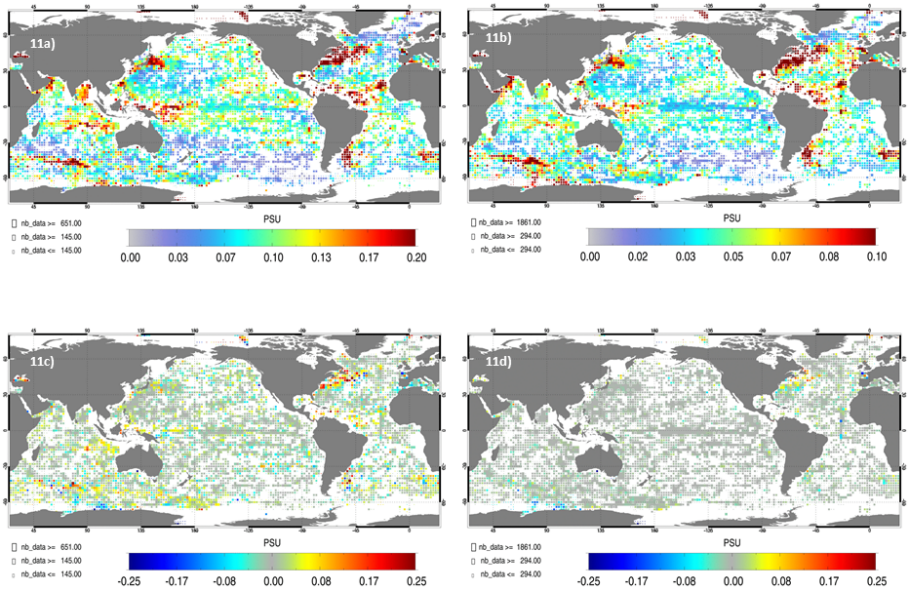

Figure 11. Spatial distribution of the RMS and the mean salinity differences between Run-Ref and in situ observations in the 0–300 and 700–2000 m layers: **(a)** shows the RMS salinity differences in the 0–300 m layer. **(b)** shows the RMS salinity differences in the 700–2000 m layer. **(c)** shows the mean salinity differences in the 0–300 m layer. **(d)** shows the mean salinity differences in the 700–2000 m layer.

OSD
12, 1145–1186, 2015

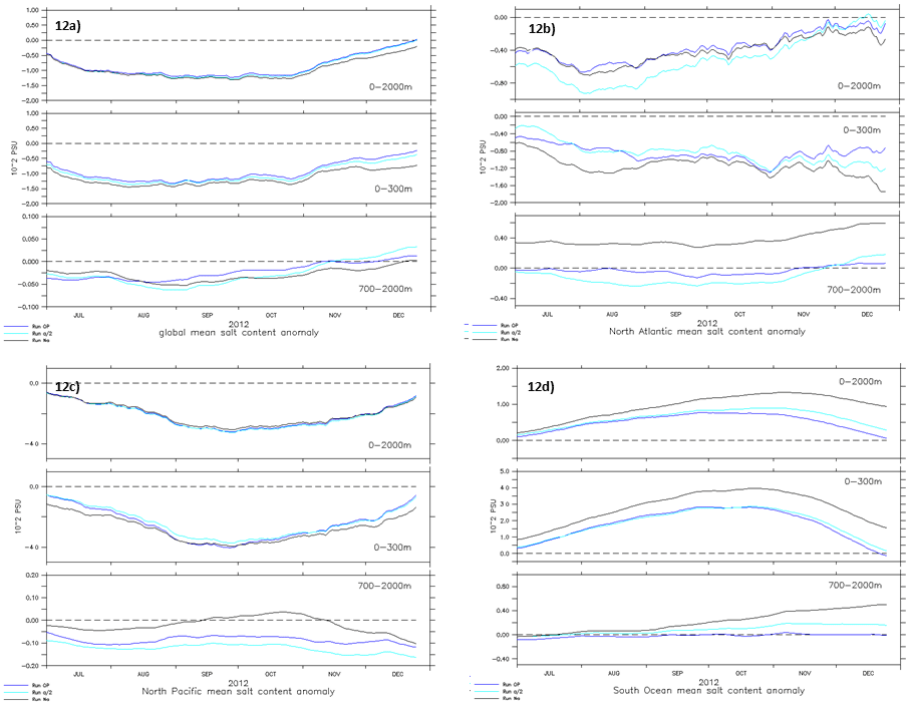

Figure 12. Salt content anomaly time series for the 0–2000, 0–300 and 700–2000 m layers for Run-Ref (blue), Run-NoArgo (black), and Run-Argo2 (light blue) and for the Global Ocean **(a)**, North Atlantic Ocean **(b)**, North Pacific Ocean **(c)**, and Southern Ocean **(d)**.

OSD
12, 1145–1186, 2015

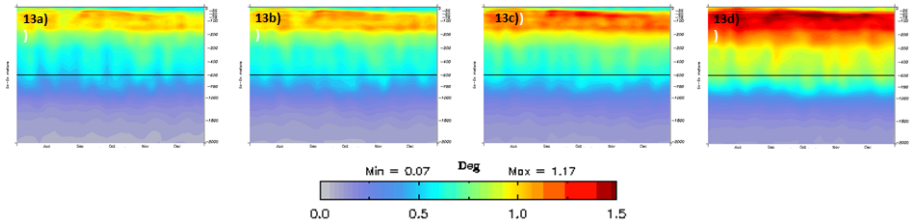

Figure 13. RMS time series of the temperature innovations for Run-Ref **(a)**, Run-Argo2 **(b)**, Run-NoArgo **(c)** and Free Run **(d)**.

OSD
12, 1145–1186, 2015

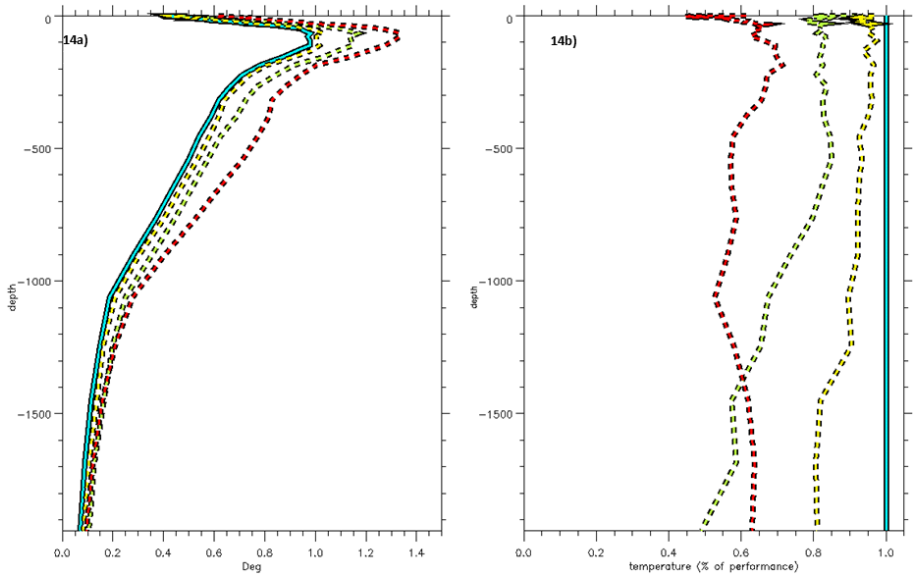

Figure 14. Vertical structure of RMS of temperature innovations **(a)** and normalized RMS of temperature innovations **(b)** from 0–2000 m for Run-Ref (blue), Run-Argo2 (yellow), Run-NoArgo (green) and Free Run (red).

OSD
12, 1145–1186, 2015

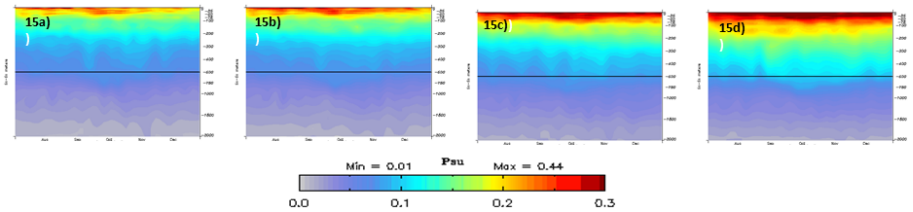

Figure 15. RMS time series of the salinity forecast field and in situ salinity differences for Run-Ref **(a)**, Run Argo2 **(b)**, Run-NoArgo **(c)** and Free Run **(d)**.

OSD
12, 1145–1186, 2015

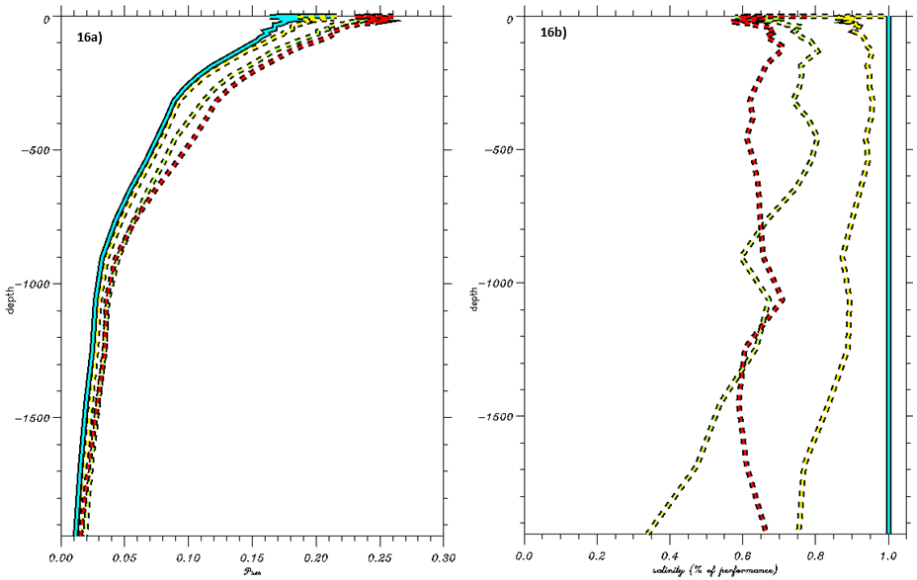

Figure 16. Vertical structure of RMS of salinity innovations **(a)** and normalized RMS of salinity innovations **(b)** from 0–2000 m for Run-Ref (blue), Run-Argo2 (yellow), Run-NoArgo (green) and Free Run (red).

OSD
12, 1145–1186, 2015